J|A|C|S
ARTICLES
Published on Web 03/23/2006

Simulating FRET from Tryptophan: Is the Rotamer Model Correct?

Frank R. Beierlein,[†] Olaf G. Othersen,[†] Harald Lanig,[†] Siegfried Schneider,[‡] and Timothy Clark*,[†]

Contribution from the Computer-Chemie-Centrum, Friedrich-Alexander-Universität Erlangen-Nürnberg, Nägelsbachstrasse 25, 91052 Erlangen, Germany, and Institut für Physikalische und Theoretische Chemie, Friedrich-Alexander-Universität Erlangen-Nürnberg, Egerlandstrasse 3, 91058 Erlangen, Germany

Received December 12, 2005; E-mail: clark@chemie.uni-erlangen.de

Abstract: We present a computational model study designed to simulate the results of time-resolved fluorescence spectra of tryptophan in proteins. In such measurements, the occurrence of more than one fluorescence lifetime is generally attributed to the existence of several tryptophan rotamers and/or structural conformations of the protein structure. The protein system we chose for this initial study is the tetracycline repressor (TetR), an interesting model system for the investigation of the mechanisms of transcriptional regulation. Fluorescence resonance energy transfer (FRET) from tryptophan to tetracycline is frequently observed in complexes of the TetR with the antibiotic tetracycline. We use a combined classical/quantum mechanical approach to model the structure and the spectroscopic properties of the TetR−tetracycline complex. A classical molecular dynamics simulation provides input geometries for semiempirical quantum mechanical/molecular mechanical (QM/MM) single-point configuration interaction (CI) calculations, which are used to calculate tryptophan vertical absorption and fluorescence energies and intensities as well as relative FRET rate constants. These rate constants together with the Einstein coefficients for spontaneous emission and an assumed rate for nonradiative deactivation allow us to simulate fluorescence decay curves with and without FRET and for the entire ensemble as well as for individual rotamers. Our results indicate that the classical "rotamer model", used to explain the multiexponential fluorescence-decay curves of time-resolved tryptophan emission spectra, can be extended to systems with FRET acceptors present in the protein matrix but that the interpretation of the fitted lifetimes is different to that usually used.

Introduction

Tetracycline (Tc) and its derivatives form a family of widely used broad-spectrum antibiotics that show bacteriostatic activity against Gram-positive and Gram-negative bacteria and other infective pathogens such as ricketsiae, mycoplasms, viruses, and protozoans. The tetracycline repressor/operator (TetR/*tetO)* system is a regulatory switch in the most important resistance mechanism of Gram-negative bacteria against the tetracycline class of antibiotics. When tetracycline enters the bacterial cell, it forms a chelate complex with divalent metal ions, mostly Mg^{2+}. Under physiological conditions, the metal cation is chelated by the deprotonated 1,3-keto−enol group O11/O12$^-$ of the zwitteranionic tetracycline molecule (Chart 1).[1−5]

Chart 1. Structure of the Physiologically Active Tetracycline−Magnesium Complex[1−3] [a]

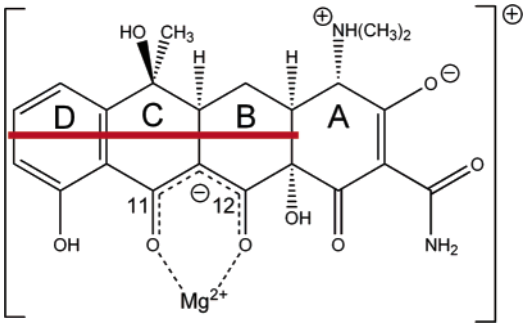

[a] The red line shows the orientation of the transition dipole of the first intense absorption in the BCD chromophore.

The expression of the protein responsible for the resistance, the tetracycline antiporter (TetA), is under tight transcriptional control of TetR. TetA is an intrinsic membrane transport protein that acts as an antiporter across the cell membrane and couples the efflux of the $[TcMg]^+$ complex with the uptake of H^+. In the absence of Tc, homodimeric TetR binds specifically to two operator sequences of the DNA *(tetO)* and thus prevents the expression of the genes *tetA* and *tetR*, i.e., the genes coding

[†] Computer-Chemie-Centrum.
[‡] Institut für Physikalische und Theoretische Chemie.

(1) Saenger, W.; Orth, P.; Kisker, C.; Hillen, W.; Hinrichs, W. *Angew. Chem.* **2000**, *112*, 2122−2133.
(2) Saenger, W.; Orth, P.; Kisker, C.; Hillen, W.; Hinrichs, W. *Angew. Chem., Int. Ed.* **2000**, *39*, 2042−2052.
(3) Hinrichs, W.; Fenske, C. In *Tetracyclines in Biology, Chemistry and Medicine*; Nelson, M., Hillen, W., Greenwald, R. A., Eds.; Birkhäuser Verlag: Basel, Boston, Berlin, 2001; pp 107−123.
(4) Othersen, O. G.; Beierlein, F.; Lanig, H.; Clark, T. *J. Phys. Chem. B* **2003**, *107*, 13743−13749.
(5) Othersen, O. G.; Lanig, H.; Clark, T. *J. Med. Chem.* **2003**, *46*, 5571−5574.

10.1021/ja058414l CCC: $33.50

itself and the TetA protein. Two molecules of the $[TcMg]^+$ complex bind to the TetR binding sites. This induces a cascade of allosteric conformational changes in the TetR protein, which result in an increased center-to-center separation of the DNA-recognition helices (from 36.6 Å in the operator complex to 39.6 Å after inducer binding).[1−3] These conformational changes lead to the dissociation of the TetR/DNA complex.

One of the most useful spectroscopic techniques for the analysis of biopolymers in action and interaction uses *fluorescence resonance energy transfer* (FRET).[6−13] This nonradiative energy transfer from a donor (D) to an acceptor (A) chromophore was first described by Theodor Förster in 1948.[6,7] The basic requirements for FRET are sufficient overlap of the donor emission spectrum and the absorption spectrum of the acceptor, proximity of donor and acceptor (D−A separation 10−100 Å), and an almost parallel orientation of their transition dipoles. Because of its strong distance dependency, FRET is frequently used to examine molecular distances in biological macromolecules ("spectroscopic ruler"[13]), an important technique for the observation of molecular interactions and conformational changes (e.g., protein folding) with high spatial (1−10 nm) and time (<1 ns) resolutions. It can be combined with single-molecule detection techniques, even in vivo.[10] In addition to these applications, FRET is also used in molecular diagnostics, e.g., in the "real-time polymerase chain reaction".[10] "Molecular beacons"[14,15] and "scorpion oligonucleotides"[16] are used for quantitative nucleic-acid detection.[10] The activity of proteins has also been monitored by FRET techniques.[10]

Protein fluorescence is caused by the three aromatic amino acids tryptophan (Trp, W), tyrosine (Tyr, Y), and phenylalanine (Phe, F). The dominant fluorophore, tryptophan, has complex spectroscopic properties. Its emission spectrum is very sensitive to its local environment and fluorescence quenchers. Complex time-resolved fluorescence decays are even found for tryptophan itself, as well as for proteins that contain only a single tryptophan residue. Such proteins show mostly multiexponential intensity-decay curves. The emission maximum of tryptophan in water occurs near 350 nm and depends strongly on the polarity and local environment.[9]

Another complicating factor is the existence of two nearly isoenergetic excited singlet states called ^1L_a and ^1L_b. Depending on the environment, either of these states can have the lower energy, although ^1L_a is usually S_1. According to Kasha's rule, and if the S_1-S_2 energy separation is large enough, the lowest-energy state is the emitting one. The transition dipoles for the ^1L_a and ^1L_b transitions are oriented almost perpendicular to each other (Chart 2). Tryptophan emission in solution and most proteins is unstructured and takes place from the ^1L_a state.[9] Compared to ^1L_b, the ^1L_a transition has a sizable charge transfer (CT) component, with lower electron density than the ground state on atoms 1 and 3 and higher on atoms 4, 7, and 9 (see Chart 2). The resulting increase in the permanent dipole moment is calculated to be 3−5 D, with the pyrrole ring becoming more positive.[17] This dipole change causes the tryptophan ^1L_a transition to be very solvent sensitive.[17,18]

Chart 2. Transition Dipoles Between the Ground State, ^1L_a[a] and ^1L_b[a] in Tryptophan

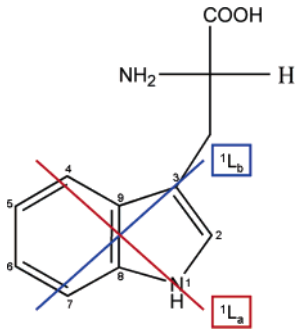

[a] Red and blue, respectively, adapted from ref 9, 17.

Time-resolved protein fluorescence intensity-decay curves are sensitive to bound ligands or other binding partners that affect the mobility of tryptophan, displace tryptophan residues to new locations, or act as quenchers or energy acceptors in a resonance-energy-transfer process.[9]

The fluorescence decay of tryptophan in neutral aqueous solution is known to be biexponential, with decay times of 3.1 and 0.51 ns.[9,19] Early work explained these two decay times by simultaneous emissions from both the ^1L_a and the ^1L_b excited states.[20] However, today there is consensus that the biexponential decay results from the presence of rotational isomers (rotamers)[9,19,21,22] and that tryptophan, unless in a completely nonpolar environment, only emits from its ^1L_a state.[9]

In a protein, the effect of the charged ammonium group, which determines the fluorescence behavior of tryptophan itself in aqueous solution,[9,19,21,22] is no longer relevant. A model compound frequently used, *N*-acetyl-L-tryptophanamide (NATA), has essentially the same structure as nonterminal tryptophan residues in proteins. The fluorescence decay of NATA is essentially monoexponential,[9,21,23] with a lifetime of ∼3.0 ns in water at pH 7.[9,19,21] Fluorescence decays of tryptophan in proteins are typically complex and are usually fitted with two or more exponential functions. Even most single-tryptophan proteins have bi or triexponential decays. Known exceptions are, e.g., apoazurin from *Pseudomonas fluorescens*[24] and, under certain conditions, ribonuclease T_1 (RNase T_1) from *Aspergillus oryzae*,[9] which are monoexponential.

The origin of multiexponential decay curves in single-tryptophan proteins is a result of protein structure, such as multiple protein conformations. As amino acids near the emitting tryptophan can quench its fluorescence, different backbone conformations result in different decay times. However, multi-

(6) Förster, T. *Z. Naturforsch., A: Phys. Sci.* **1949**, *4*, 321−327.
(7) Förster, T. *Ann. Phys. (Leipzig)* **1948**, *2*, 55−75.
(8) Stryer, L. *Annu. Rev. Biochem.* **1978**, *47*, 819−846.
(9) Lakowicz, J. R. *Principles of Fluorescence Spectroscopy*, 2nd ed.; Kluwer Academic/Plenum Publishers: New York, 1999.
(10) Brakmann, S.; Nöbel, N. *Nachr. Chem.* **2003**, *51*, 319−323.
(11) Dale, R. E.; Eisinger, J. *Proc. Natl. Acad. Sci. U.S.A.* **1976**, *73*, 271−273.
(12) Dos Remedios, C. G.; Moens, P. D. J. *J. Struct. Biol.* **1995**, *115*, 175−185.
(13) Stryer, L.; Haugland, R. P. *Proc. Natl. Acad. Sci. U.S.A.* **1967**, *58*, 719−726.
(14) Summerer, D.; Marx, A. *Angew. Chem.* **2002**, *114*, 3778−3780.
(15) Summerer, D.; Marx, A. *Angew. Chem., Int. Ed.* **2002**, *41*, 3620−3622.
(16) Thelwell, N.; Millington, S.; Solinas, A.; Booth, J.; Brown, T. *Nucleic Acids Res.* **2000**, *28*, 3752−3761.
(17) Callis, P. R. In *Methods in Enzymology*; Brand, L., Johnson, M. L., Eds.; Academic Press: San Diego, New York, Boston, London, Sydney, Tokyo, Toronto, 1997; Vol. 278, pp 113−150.
(18) Vivian, J. T.; Callis, P. R. *Biophys. J.* **2001**, *80*, 2093-2109.
(19) Szabo, A. G.; Rayner, D. M. *J. Am. Chem. Soc.* **1980**, *102*, 554−563.
(20) Rayner, D. M.; Szabo, A. G. *Can. J. Chem.* **1978**, *56*, 743−745.
(21) Petrich, J. W.; Chang, M. C.; McDonald, D. B.; Fleming, G. R. *J. Am. Chem. Soc.* **1983**, *105*, 3824−3832.
(22) Creed, D. *Photochem. Photobiol.* **1984**, *39*, 537−562.
(23) Zelent, B.; Kusba, J.; Gryczynski, I.; Johnson, M. L.; Lakowicz, J. R. *Biophys. Chem.* **1998**, *73*, 53−75.
(24) Hutnik, C. M.; Szabo, A. G. *Biochemistry* **1989**, *28*, 3935−3939.

exponential decay curves are even observed when a protein is assumed to be in a single backbone conformation.[9] In these cases, tryptophan multiexponential decay in proteins is usually attributed to the existence of multiple ground-state conformers of the tryptophan side chain.[25] Similar to tryptophan in solution, the "rotamer model" is also used to explain fluorescence decays of tryptophan residues in proteins. Each conformation has a different microenvironment, leading to a distinct nonradiative decay rate because of different distances and relative orientations to quencher groups.[19,21,25] Possible tryptophan-quenching pathways that are sensitive to environment are excited-state electron and proton transfers and solvent quenching.[25] Charge transfer from the excited indole moiety to the carbonyl group of the peptide bond is probably the main nonradiative quenching pathway of tryptophan in proteins.[21,25] Histidine residues can quench tryptophan fluorescence by charge-transfer (CT) or proton-transfer mechanisms.[25] Many studies explain multiexponential tryptophan-fluorescence decays in proteins on the basis of the rotamer model or its modifications.[25−33] Alternatives to the rotamer model invoke spectral migration due to structural relaxation of the surrounding protein.[26,34,35]

A representative example of a protein with FRET quenching of tryptophan is the tetracycline-repressor/tetracycline complex, where the bound inducer tetracycline acts as an energy acceptor. In the present study, we show how multiexponential tryptophan fluorescence decay is obtained from a molecular dynamics (MD) trajectory containing two tryptophan rotamers by calculating the FRET rate constant for every MD snapshot.

Tryptophan 43 (Trp43, W43), situated in the DNA-binding domain of the tetracycline repressor, is frequently used as a probe for exploring the conformation of the protein in time-resolved fluorescence measurements of TetR.[25,27,29,30] The fluorescence-decay curves obtained from these measurements are usually fitted using two or three exponential functions, suggesting that two or three species with different fluorescence lifetimes are present.[25,27,29,30] Usually, these different tryptophan species are interpreted in the framework of the "rotamer model", which assigns the two−three lifetimes found for Trp to two−three discrete rotamers of this residue.[25,27,29] Some of the published experimental studies have used molecular mechanics (MM) to assign Trp rotamers to the lifetimes observed experimentally.[25,28]

In the following, we have investigated the complex formed between class D TetR and tetracycline.[36] The experimental analogue to our model is the complex formed by the single-tryptophan TetR mutant W75F, for which a biexponential Trp decay with lifetimes of 2.55 and 0.42 ns has been reported.[27]

The existing models for the interpretation of TetR spectroscopic data are largely speculative, so that conclusions for the induced tetracycline repressor (TetR) must be validated by computer simulations to confirm the interpretation of the experimental results. Therefore, we have used a combined molecular dynamics−QM/MM approach that allows us to calculate vertical absorption and fluorescence energies and intensities as well as fluorophore quenching by FRET.[37−42]

Methods

A classical molecular dynamics simulation, for which we use the AMBER[43−45] program, gives "hot" geometries of a protein, which are the basis for combined quantum mechanical/molecular mechanical (QM/MM) single-point configuration interaction (CI) calculations using the semiempirical program package VAMP.[46,47] The relevant chromophores are embedded in the protein environment and the solvent using a QM/MM CI approach in which the environment is represented by a classical force field. The polarization of the QM wave function by the point charges in the MM environment is taken into account via an additional one-electron term in the Fock matrix.[48−50]

The semiempirical CI calculations provide all the variables necessary to calculate both the absorption and fluorescence wavelengths and intensities and the FRET energy-transfer probabilities according to Förster theory,[6−9] as shown in the Supporting Information. In our simulation, the properties of a bulk system that in reality consists of a large number of molecules are simulated by analyzing the temporal evolution of a single-protein test system. This resembles the ensemble model of bulk fluorescence properties from single-molecule measurements described by Hochstrasser, Lee, and Tang.[51]

Recently, classical molecular dynamics simulations have been used increasingly for simulating FRET.[52−55] In these studies, the MD force

(25) Antonini, P. S.; Hillen, W.; Ettner, N.; Hinrichs, W.; Fantucci, P.; Doglia, S. M.; Bousquet, J.-A.; Chabbert, M. *Biophys. J.* **1997**, *72*, 1800−1811.
(26) Marian, D.-T.; Leypold, C.; Kunz, M.; Schneider, S.; Schubert, P.; Scholz, O.; Hillen, W. *Photochem. Photobiol. Sci.* **2002**, *1*, 841−851.
(27) Kaszycki, P.; Guz, A.; Drwiega, M.; Wasylewski, Z. *J. Protein Chem.* **1996**, *15*, 607−619.
(28) Kunz, M.; Kintrup, M.; Hillen, W.; Schneider, S. *Photochem. Photobiol.* **2000**, *72*, 35−48.
(29) Peviani, C.; Hillen, W.; Ettner, N.; Lami, H.; Doglia, S. M.; Piémont, E.; Ellouze, C.; Chabbert, M. *Biochemistry* **1995**, *34*, 13007−13015.
(30) Chabbert, M.; Hillen, W.; Hansen, D.; Takahashi, M.; Bousquet, J.-A. *Biochemistry* **1992**, *31*, 1951−1960.
(31) Sillen, A.; Hennecke, J.; Roethlisberger, D.; Glockshuber, R.; Engelborghs, Y. *Proteins: Struct., Funct., Genet.* **1999**, *37*, 253−263.
(32) Sillen, A.; Díaz, J. F.; Engelborghs, Y. *Protein Sci.* **2000**, *9*, 158−169.
(33) Martinho, J. M. G.; Santos, A. M.; Fedorov, A.; Baptista, R. P.; Taipa, M. A.; Cabral, J. M. S. *Photochem. Photobiol.* **2003**, *78*, 15−22.
(34) Toptygin, D.; Savtchenko, R. S.; Meadow, N. D.; Brand, L. *J. Phys. Chem. B* **2001**, *105*, 2043−2055.
(35) Toptygin, D.; Brand, L. *Chem. Phys. Lett.* **2000**, *322*, 496−502.
(36) Hinrichs, W.; Kisker, C.; Düvel, M.; Müller, A.; Tovar, K.; Hillen, W.; Saenger, W. *Science (Washington, D.C.)* **1994**, *264*, 418−420.
(37) Beierlein, F. Ph.D. Thesis, Universität Erlangen-Nürnberg, Erlangen, Germany, 2005.
(38) Beierlein, F.; Clark, T. In *High Performance Computing in Science and Engineering*, Transactions of the Second Joint HLRB and KONWIHR Status and Result Workshop, Technical University of Munich and Leibnitz-Rechenzentrum Munich, Munich, Germany, March 2−3, 2004; Wagner, S., Hanke, W., Bode, A., Durst, F., Eds.; Springer-Verlag: Berlin, Heidelberg, New York, 2004; pp 245−260.
(39) Beierlein, F.; Lanig, H.; Othersen, O.; Schneider, S.; Clark, T. *An MD/CI-approach simulating FRET in proteins*, 227th ACS National Meeting, Anaheim, CA, United States, March 28−April 1, 2004.
(40) Beierlein, F.; Lanig, H.; Othersen, O.; Schneider, S.; Clark, T. *An MD/CI Approach for the Investigation of Fluorescence Resonance Energy Transfer in Proteins*, 17. Darmstädter Molecular Modelling Workshop, Erlangen, Germany, May 27−28, 2003.
(41) Lanig, H.; Beierlein, F.; Othersen, O.; Schneider, S.; Clark, T. *Combining Molecular Dynamics Simulations with Semiempirical CI−Calculations to Investigate Fluorescence Resonance Energy Transfer (FRET) within the Tetracycline Repressor*, 43rd Sanibel Symposium, St. Augustine, Florida, February 22−March 1, 2003.
(42) Beierlein, F.; Othersen, O.; Clark, T.; Lanig, H. *A Molecular Dynamics/Configuration Interaction (MD/CI)-Approach Simulating FRET in Proteins*, eCheminfo 2004 "Applications of Cheminformatics and Modelling to Drug Discovery", http://echeminfo.colayer.net, November 8−19, 2004.
(43) Case, D. A., et al. *AMBER 8*, University of California: San Francisco, 2004.
(44) Case, D. A., et al. *AMBER 7*, University of California: San Francisco, 2002.
(45) Case, D. A., et al. *AMBER 5*, University of California: San Francisco, 1997.
(46) Clark, T., et al. *VAMP 8.1*, Computer-Chemie-Centrum, Universität Erlangen-Nürnberg: Erlangen, Germany, 2002.
(47) *MS Modeling 3.0.1*, Accelrys Inc.: San Diego, CA, 2003.
(48) Rauhut, G.; Clark, T.; Steinke, T. *J. Am. Chem. Soc.* **1993**, *115*, 9174−9181.
(49) Clark, T.; Alex, A.; Beck, B.; Gedeck, P.; Lanig, H. *J. Mol. Model.* **1999**, *5*, 1−7.
(50) Gedeck, P.; Schneider, S. *J. Photochem. Photobiol., A* **1997**, *105*, 165−181.
(51) Lee, M.; Tang, J.; Hochstrasser, R. M. *Chem. Phys. Lett.* **2001**, *344*, 501−508.
(52) Ortiz, W.; Roitberg, A. E.; Krause, J. L. *J. Phys. Chem. B* **2004**, *108*, 8218−8225.

field represented the electronic ground state, and the force field was not adapted to the excited state (in contrast to the work of Callis and Vivian[18]), and the transition dipoles were not calculated quantum mechanically for every MD snapshot, as in this work.

Molecular Dynamics Simulations. The details of preparation of the protein structure and of the MD protocol are given in the Supporting Information.

The trajectory was processed and analyzed with Ptraj 6.5.[56] To remove protein rotation, the whole trajectory was fitted on the minimized X-ray structure (only C_α atoms were used for fitting and RMSD calculation). For assessing protein stability in the MD production phase, an average structure of all production-phase snapshots was calculated using Ptraj and compared with the X-ray structure. For QM/MM input generation, we processed all snapshot geometries with Ptraj so that the water box was centered on Asp53. This was necessary to obtain structures with the QM parts (Trp43 and Tc) roughly in the center of the QM/MM system. The monomers were calculated separately in the QM/MM part of the protocol (i.e., intermonomer FRET was ignored, see Supporting Information).

Semiempirical CI Calculations. The 7093 snapshots collected during the production phase were used for the semiempirical CI single-point calculations. Two different sets of QM/MM CI calculations with VAMP 8.1[46] using the AM1 Hamiltonian[57] were performed for each monomer of TetR, one of them with the donor and the other with the acceptor in the QM part. The MM environment was represented by a rigid point-charge environment.[49,50] MM charges were taken from the AMBER 1994 force field.[58] The polarization of the QM wave function by the point charges in the MM environment was taken into account via an additional one-electron term in the Fock matrix.[48−50] No back-polarization of the MM part by the QM part was included. As explicit solvent molecules were present, we used a constant dielectric constant of 1.0 for both the MM− and the QM/MM−Coulomb interactions. For more details of the QM/MM implementation, see refs 49, 50, and 59−62.

We defined tetracycline together with the magnesium ion as the QM part in the set of calculations for the FRET acceptor tetracycline, giving a good representation of the electronic properties of the chromophore. The QM part with Tc and Mg^{2+} consisted of 65 atoms, which were surrounded by 34 576 MM atoms.

In the case of the CI calculations of the FRET donor tryptophan, the protein backbone was cut for QM input generation. The process used to decide on the most appropriate cutting scheme is described in the Supporting Information. In the CI calculations for the FRET donor chromophore, the 44 QM atoms of the Gly-Trp-Gly fragment were embedded in 34 597 MM atoms. An active space of 26 orbitals symmetrically distributed around the HOMO−LUMO border was used. Single and pair-double excitations were considered in the CI.[63] For all donor and acceptor snapshots, the transition dipoles for all $S_0 \rightarrow S_i$ transitions were calculated. This procedure led to a total of 28 372 QM/MM CI calculations.

For a validation of our approach, we performed a short MD simulation of zwitterionic glycyltryptophan (Gly-Trp, GW) in water, as described in the Supporting Information. Snapshots from this simulation were used for analogous AM1/CI single-point calculations to those used for the protein simulations. Glycyltryptophan was chosen as the QM part, whereas the water molecules formed the MM part. MM charges were taken from the force field used in the AMBER MD simulation.[58] Another set of QM calculations considered the influence of the surrounding solvent using the self-consistent reaction field (SCRF) technique as described by Rauhut, Clark, and Steinke.[48]

Absorption and Emission Profiles. The details of the calculation of absorption and emission profiles are given in the Supporting Information; thus, we will only outline the major assumptions here. Vertical absorption and emission wavelengths were calculated. For the simulation of steady-state and time-resolved fluorescence transitions, we calculated the Einstein coefficient of spontaneous emission A_{nm} for each snapshot from the transition moment and the wavelength of the transition.

Steady-state fluorescence profiles (i.e., the sums of the calculated vertical transitions) of the whole ensemble/the whole MD trajectory were calculated with a binned resolution of 0.1 nm. The profiles were constructed by plotting the sums of the A_{nm} values in each bin vs the emission wavelengths, λ.

To obtain time-resolved fluorescence decays, the time-dependent fluorescence intensity was calculated by summation over all MD snapshots, assuming for each snapshot a first-order decay of the Trp S_1 state. Nonradiative processes were approximated as having a single, constant rate, and excited-state relaxation was ignored throughout.

Absorption spectra were generated analogously to the steady-state fluorescence profile by plotting the sums of the oscillator strengths for a given wavelength vs the wavelength. All transitions $S_0 \rightarrow S_i$ in all snapshots were considered. Wavelength data were calculated for the vertical transition between S_0 and the target states. This approach neglects Franck−Condon effects completely and, therefore, gives narrower profiles than the bands observed in the experimental spectra.

Fluorescence-Resonance-Energy-Transfer (FRET) Probabilities. Again, full details of the calculations of FRET probabilities are given in the Supporting Information. The FRET probability is calculated using standard Förster theory based on interactions between the calculated transition dipoles of the two chromophores taken from the snapshots. The total rate constant for donor deactivation with FRET quenching is given by the sum of the rate constant for the donor fluorescence, calculated from the Einstein coefficients, the rate for nonradiative decay, which is assumed to be constant and to have a value compatible with the experimental results, and the calculated FRET rate.

The FRET rate depends on the distance between the chromophores and the orientation factor κ^2, which describes the relative orientation of the donor and the acceptor transition dipoles. If the donor and acceptor rotate freely (e.g., in isotropic solution), the mean value of κ^2 is 2/3, a value assumed in many studies. This value is appropriate for solution studies of small molecules but not for molecules bound to proteins, which have very anisotropic orientational distributions.

Only Trp emission from the S_1 state was considered. The choice of acceptor transition is more difficult as the resonance condition is not defined within our model, which does not consider excited-state relaxation. We therefore used an energy-difference cutoff to determine which acceptor transitions to consider, as outlined in detail in the Supporting Information. To convert the calculated relative FRET rate constants for the snapshots into realistic absolute rates, we used a factor $A = 7.69 \times 10^{17}$ to obtain a rate constant distribution with a mean k_T value of 2×10^8 s^{-1}, a value that follows from experimental investigations.[26,28,64−66] Each of the snapshots decays according to a first-order law. Therefore, we can express the time-dependent fluo-

(53) Stultz, C. M.; Levin, A. D.; Edelman, E. R. *J. Biol. Chem.* **2002**, *277*, 47653−47661.
(54) Laboulais, C.; Deprez, E.; Leh, H.; Mouscadet, J.-F.; Brochon, J.-C.; Le Bret, M. *Biophys. J.* **2001**, 473−489.
(55) Gustiananda, M.; Liggins, J. R.; Cummins, P. L.; Gready, J. E. *Biophys. J.* **2004**, *86*, 2467−2483.
(56) Cheatham, T. E., III *Ptraj 6.5*, University of Utah: Salt Lake City, Utah, 2003.
(57) Dewar, M. J. S.; Zoebisch, E. G.; Healy, E. F.; Stewart, J. J. P. *J. Am. Chem. Soc.* **1985**, *107*, 3902−3909.
(58) Cornell, W. D., et al. *J. Am. Chem. Soc.* **1995**, *117*, 5179−5197.
(59) Schürer, G.; Horn, A. H. C.; Gedeck, P.; Clark, T. *J. Phys. Chem. B* **2002**, *106*, 8815−8830.
(60) Beierlein, F.; Lanig, H.; Schürer, G.; Horn, A. H. C.; Clark, T. *Mol. Phys.* **2003**, *101*, 2469−2480.
(61) Schürer, G.; Lanig, H.; Clark, T. *J. Phys. Chem. B* **2000**, *104*, 1349−1361.
(62) Schürer, G.; Lanig, H.; Clark, T. *Biochemistry* **2004**, *43*, 5414−5427.
(63) Clark, T.; Chandrasekhar, J. *Isr. J. Chem.* **1993**, *33*, 435−448.
(64) Kintrup, M.; Schubert, P.; Kunz, M.; Chabbert, M.; Alberti, P.; Bombarda, E.; Schneider, S.; Hillen, W. *Eur. J. Biochem.* **2000**, *267*, 821−829.
(65) Kunz, M. Ph.D. Thesis, Universität Erlangen-Nürnberg, Erlangen, Germany, 2000.
(66) Roman, C. Ph.D. Thesis, Universität Erlangen-Nürnberg, Erlangen, Germany, 2005.

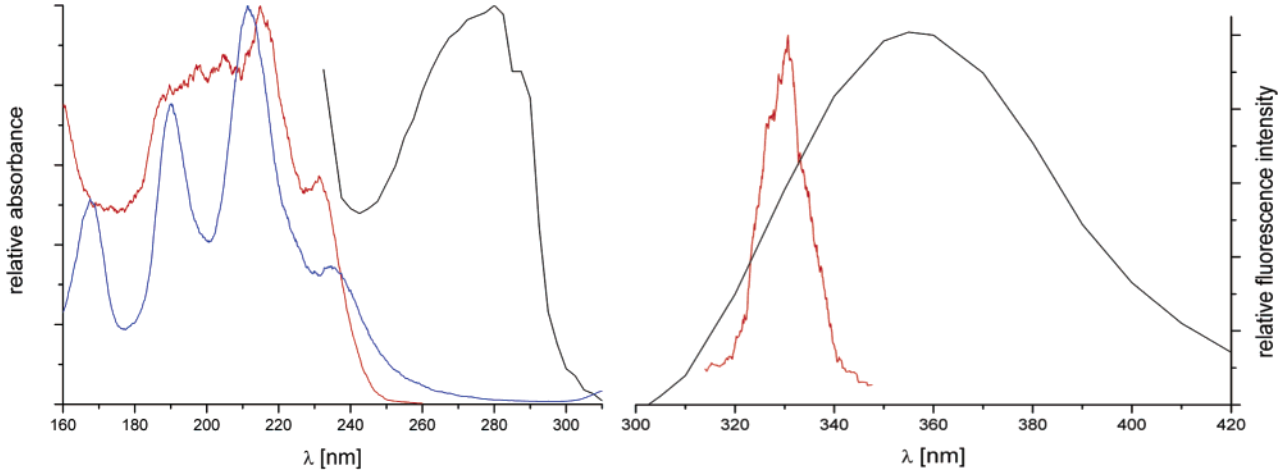

Figure 1. Summed calculated absorption (SCRF: red, QM/MM: blue) and fluorescence (only SCRF: red, see text) vertical transitions (from and to the ground-state geometry of the snapshots) for the zwitterionic glycyltryptophan ensemble and the experimental[9] (black) absorption (left) and fluorescence (right) spectra of tryptophan in aqueous solution (pH = 7). The calculated absorption and emission data were smoothed by averaging 50 (absorption) and 20 (emission) adjacent data points.

rescence intensity by summation over all snapshots. The decay curves thus calculated were fitted with sums of exponential functions to obtain relative ensemble lifetimes as described in the Supporting Information.

Results and Discussion

Validation: Glycyltryptophan Absorption and Emission. The steady-state absorption and emission spectra (experimental) and summed vertical transitions from the simulation for zwitterionic glycyltryptophan are shown in Figure 1. Note that these plots do not include relaxation effects for the excited state and therefore represent vertical transitions at the ground-state geometries from the snapshots. The semiempirical calculations with the SCRF continuum solvent model and the QM/MM calculations in which the solvent was modeled as the MM environment give fairly similar results for the absorption spectrum. However, the QM/MM model also uses the ground-state equilibrium solvation of the MM environment for the excited state and is therefore not appropriate for fluorescence, whereas the SCRF technique can calculate equilibrium excited-state solvation.[48] We therefore only show the SCRF results for the glycyltryptophan ensemble fluorescence profile. This environment-relaxation problem is very severe for water solution but less significant in protein simulations because the protein environment cannot undergo the extensive geometrical relaxation characteristic of water. The band shapes of the experimental absorption spectra (Figure 1) are reproduced moderately well by summing the calculated vertical transitions. However, the simulated absorption profile is blue-shifted by about 60 nm. As expected, the calculated fluorescence profile consists of a narrow band at the blue end of the experimental peak. The narrowness of this summed fluorescence profile reflects the fact that it only represents vertical transitions at the ground-state geometries and neglects Franck−Condon effects and excited-state relaxation completely. The effect of these relaxation processes would be to broaden and red-shift the emission so that our results are probably quite accurate for the fluorescence within the assumptions made in the calculations. The blue-shifts of the calculated absorption profile relative to the experimental spectrum can be attributed to the neglect of dispersion shifts in the theory. For future work, we have now developed a

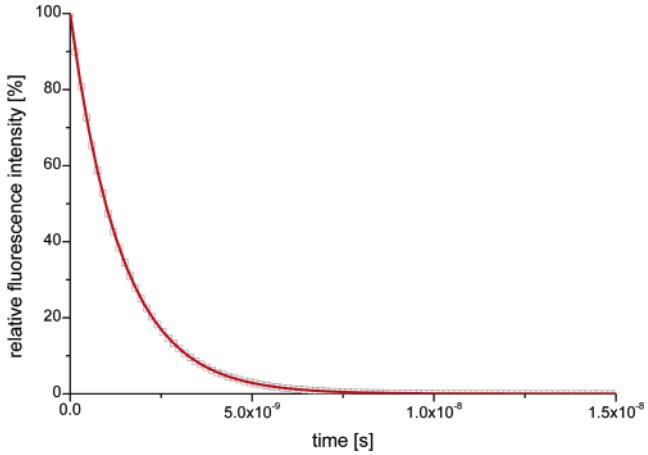

Figure 2. Simulated fluorescence decay for zwitterionic glycyltryptophan in water. Red: fitting curve (monoexponential), gray boxes: actual data points of the simulated decay (only every 100th data point shown for clarity). A value of 7×10^8 s^{-1} was assumed for k_{nr} to give approximately the correct overall decay kinetics.[21,68]

calculational technique to treat these dispersion interactions within a QM/MM framework.[67]

To simulate the fluorescence decay curves, we must first assign a rate to the nonradiative decay processes that form the background decay behavior that is modified by the fluorescence and FRET processes. As we cannot treat all possible deactivation processes, we have assigned an appropriate constant value to k_{nr}. The absolute values of the fitted decay times depend mostly on the assumed value of k_{nr}, which is roughly 90× faster than the calculated value for k_r. We therefore used an assumed value of 7×10^8 s^{-1} for k_{nr} to judge the effect of k_r on the observed decay curve (Figure 2). This value should give a total fluorescence decay rate similar to that observed experimentally.[21,68] Table 1 shows the results of mono, bi, and triexponential fits to the calculated data.

Table 1 shows quite clearly that the distribution of Einstein coefficients for the individual snapshots obtained from the

(67) Martin, B. Ph.D. Thesis, Universität Erlangen-Nürnberg, Erlangen, Germany, 2004.
(68) Chang, M. C.; Petrich, J. W.; McDonald, D. B.; Fleming, G. R. *J. Am. Chem. Soc.* **1983**, *105*, 3819−3824.

Table 1. Parameters Obtained from the Levenberg−Marquardt Fits (Eq 16 in the Supporting Information) of the Calculated Fluorescence Decay of Zwitterionic Glycyltryptophan in Water[a]

	number of exponentials		
parameter	1	2	3
χ_r^2	1.02×10^{-7}	1.02×10^{-7}	8.36×10^{-14}
r^2	1.00	1.00	1.00
τ_1/ns	1.41	1.41	1.41
τ_2/ns		1.41	1.41
τ_3/ns			1.39
α_1	100.00	50.00	41.17
α_2		50.00	41.17
α_3			17.67

[a] A value of 7×10^8 s^{-1} was assumed for k_{nr} to give approximately the correct overall decay kinetics.[21,68] The mean of the calculated k_r values is 7.67×10^6.

simulation does not lead to a multiexponential fitted decay curve. The fitted τ-values for one and two exponentials are identical so that the calculated decay is clearly monoexponential. Thus, the fluctuations caused by thermal movement and jostling by the solvent do not cause variations in the fluorescence intensity that would result in multiexponential fits. The observed multiexponential behavior must therefore be due to competing nonradiative processes, as also suggested by the experimental work.

FRET in the TetR System. As we were mainly interested in the parameters that influence FRET from Trp43 to Tc, we analyzed the χ_1/χ_2 side chain angle distribution of Trp43 and Trp43′ and the donor−acceptor distance between Trp43/Trp43′ and the tetracyclines in each monomer. Our simulations reveal flips to different Trp43 χ_1/χ_2 mean values in addition to fast fluctuations in the side-chain angles (Figure 3). Each "rotamer" thus represents an ensemble of structures with χ_1/χ_2 fluctuating around a characteristic mean value.

Figure 3 shows, however, that the mean lifetime of a given rotamer is significantly longer than that of the tryptophan excited state.

A cluster analysis of the χ_1 and χ_2 side-chain dihedrals with TSAR 3.3[69] indicated two clusters for monomer 1 and five clusters for monomer 2. This behavior, which we have also observed in longer (50 ns) simulations, indicates that on the time scale available for simulations, there is little or no coupling between the movements of the two monomers in TetR, so that essentially independent results are obtained for the two monomers. The structures representing the cluster centers for the two monomers are shown in Figure 4. Tetracycline did not change its conformation and binding mode over the whole trajectory.

Analysis of the donor−acceptor distance (defined as the distance between the geometrical center of the heavy atoms in the indole chromophore and that of the heavy atoms in the BCD chromophore of tetracycline) in monomer 1 shows an almost Gaussian-shaped distance distribution centered at 33.22 Å, whereas in monomer 2 the distance between Trp43′ and Tc shows a larger variation (Figure 5). One reason for the large variation of the donor−acceptor distance in monomer 2 is the presence of more Trp43 rotamers than in monomer 1. We also analyzed the distances between the Trp C^α atoms and the C_{1A} atom of tetracycline (not shown) to eliminate this difference. These data show that monomer 1 stays almost perfectly in its

(69) *TSAR 3.3*, version 3.3; Oxford Molecular Ltd.: Oxford, England, 2000.

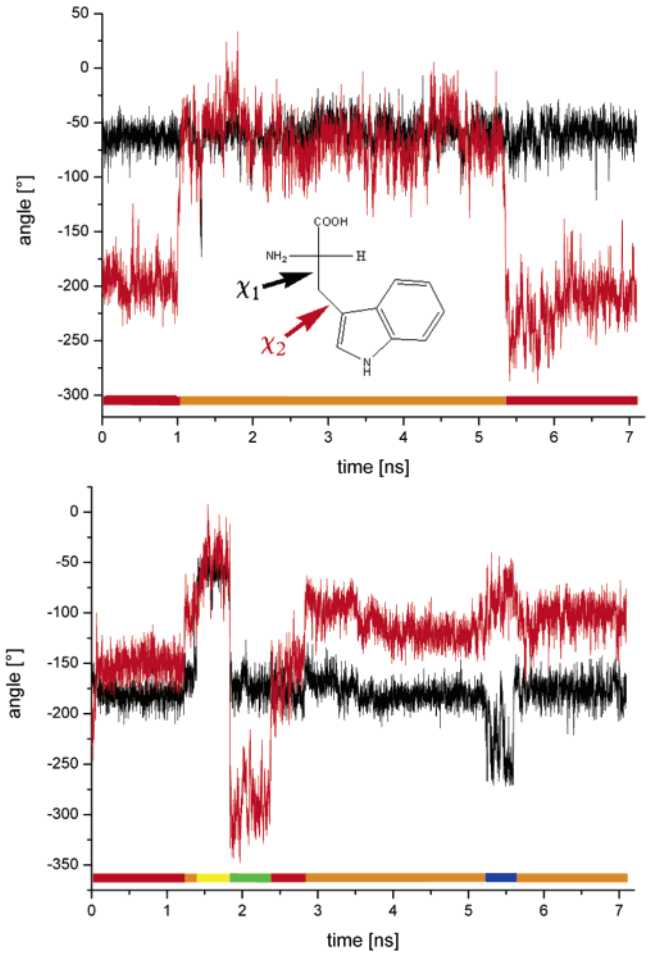

Figure 3. χ_1/χ_2 side-chain angle distribution of Trp43 (monomer 1, above) and Trp43′ (monomer 2, below). Black: χ_1, red: χ_2. Side-chain angle clusters (Figure 4) are indicated by the color-coding on the time axis.

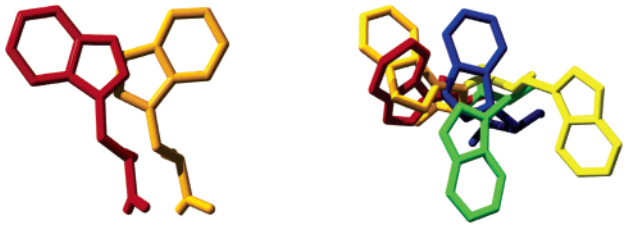

Figure 4. Trp43/Trp43′ structures representing the cluster centers for monomer 1 (left) and monomer 2 (right) obtained from a cluster analysis of the χ_1/χ_2 side chain angles. Left (monomer 1): red ($\chi_1 = -61.29°$, $\chi_2 = -209.27°$), orange ($\chi_1 = -59.14°$, $\chi_2 = -63.55°$). Right (monomer 2): red ($\chi_1 = -179.07°$, $\chi_2 = -155.72°$), orange ($\chi_1 = -176.78°$, $\chi_2 = -110.76°$), blue ($\chi_1 = -250.24°$, $\chi_2 = -74.15°$), green ($\chi_1 = -172.38°$, $\chi_2 = -288.17°$), yellow ($\chi_1 = -62.59°$, $\chi_2 = -52.07°$).

X-ray conformation, whereas in monomer 2, the DNA-binding domain (helices $\alpha_{1'}/\alpha_{2'}/\alpha_{3'}$) undergoes a small structural displacement of the protein backbone (see the Supporting Information for details of the MD results). The secondary and tertiary structures of the protein are, however, not modified in this process.

Because of the strong donor−acceptor distance-dependence of FRET, the discussion below focuses on monomer 1. However, we have also simulated the decay curves for monomer 2 separately, but not analyzed them in as much detail as the more clear-cut monomer 1. Specifically, the monomer with two, rather than five, rotamers is conceptually better suited for interpreting

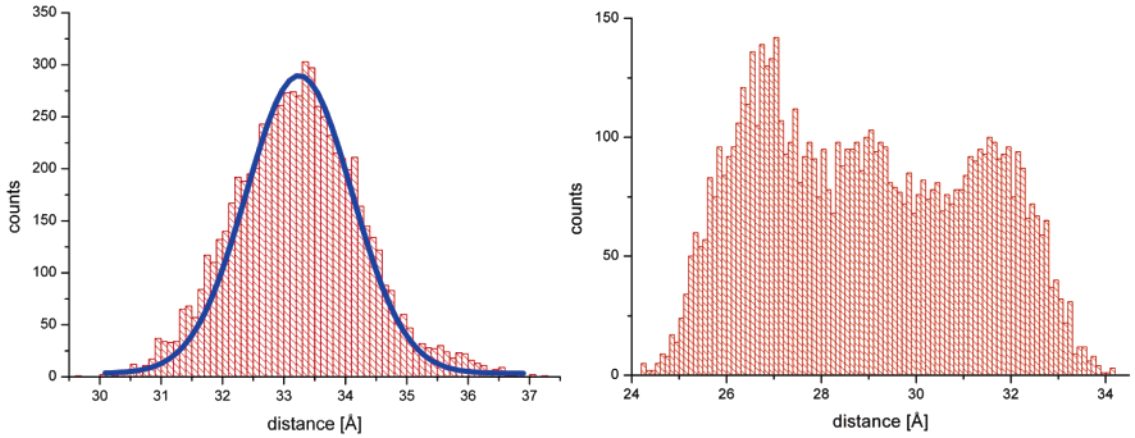

Figure 5. Distribution of distances between the geometric center of the heavy atoms in the indole chromophore (donor) and that of the heavy atoms in the BCD chromophore of tetracycline (acceptor). Left: monomer 1, right: monomer 2.

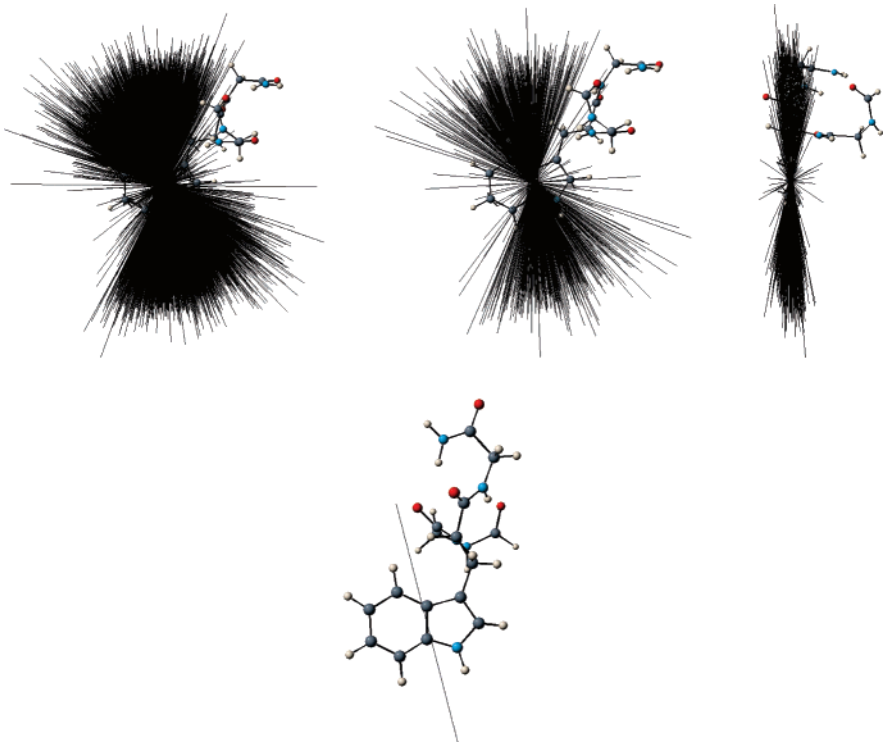

Figure 6. Calculated Trp transition dipoles for $S_0 \rightarrow S_1$. Left: All dipoles of the complete MD trajectory after fitting the indole chromophore of each snapshot on the first structure in the MD production phase. Center: Only every 10th dipole shown. Right: Every 10th dipole, side-view. Below: Structure representing the cluster center (snapshot at 3674 ps). Graphics were generated with Jmol 5.[70] The angle deviation of the transition dipole is caused by intensity borrowing between the ^1L_a and ^1L_b states induced by geometrical distortions.

experiments that give a biexponential decay for Trp43 in the TetR/Tc complex because it provides a possible direct link to a two-rotamer model.

The transition dipoles calculated for the Trp43 $S_1 \rightarrow S_0$ transition are shown in Figure 6 for all MD snapshots. The directions of the transition dipoles indicate that tryptophan emits from its ^1L_a state, although in principle geometrical relaxation could swap the order of the first two excited singlet states.

The relative orientation of the two transition dipoles involved in FRET also depends on that of the acceptor (tetracycline). Its most intense transition dipole lies in the plane of the BCD chromophore of tetracycline for each snapshot, as shown in Chart 1.

The emission profile (again, the summed vertical transitions for the ensemble) calculated for Trp43 in the protein/water box environment is shown in Figure 7. Compared with the experimental spectrum, there is a blue-shift of about 35 nm and the full width at half-maximum (fwhm) is still too small because of the neglect of the Franck−Condon factors, although it is larger than that calculated for the model system Gly-Trp.

Intrinsic Fluorescence Decay Curves. The time-resolved decays of the intrinsic fluorescence (i.e., without FRET) of Trp43 in the protein environment/water box were calculated for the whole MD trajectory (containing two rotamers) and for the two rotamers themselves. The decay curves were calculated from the Einstein coefficients A_{nm} (Figure 8) of the snapshots. They were fitted with one, two, and three exponentials, according to eq 16 in the Supporting Information. For these simulations, we assumed a rate constant of 2×10^8 s^{-1}, deduced from the

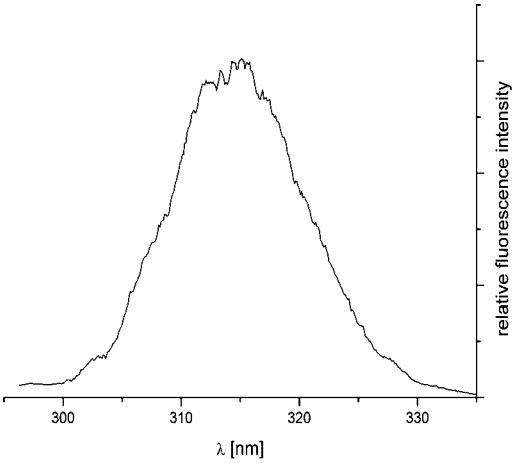

Figure 7. Calculated fluorescence profile (sum of the vertical transitions for the ensemble using the ground-state geometries from the snapshots) of Trp43, obtained from QM/MM calculations in the protein/water box environment. The approx. 15 nm blue-shift compared with the Gly-Trp simulation results from the lower polarity of the protein environment compared with water solution.

experimental results[26,28,64−66] for the nonradiative decay process in the protein environment (Figure 9).

Table 2 shows that a monoexponential fit with a fluorescence lifetime of 4.6−4.7 ns explains the decay kinetics well. Thus, this simulation, similar to that of Gly-Trp in aqueous solution, indicates that if multiexponential behavior in the absence of FRET is observed, it is not caused by variations in the fluorescence intensities due to geometrical fluctuations but rather by competing nonradiative processes. Thus, in the absence of effects such as charge transfer that might cause multiexponential behavior but were not treated explicitly here but rather approximated by a single decay-rate constant, the small fluorescence rate alone cannot cause multiexponential behavior.

Table 2 also shows that the two rotamers exhibit the same intrinsic fluorescence behavior.

The absorption profile (summed vertical transitions for the ensemble) of tetracycline in the protein binding site calculated from the QM/MM results agrees moderately well with the experimental spectrum of $[TcMg]^+$ in water (Figure 10).

The calculated Trp emission and Tc absorption profiles overlap well; thus, an important requirement for FRET is fulfilled. Although the absolute peak position and fwhm of the simulated Trp emission agree only moderately with experiment (see above), our model is not affected by this problem as it only uses the orientation factor and donor−acceptor distance as parameters for relative FRET constants.

Fluorescence Decay Curves with FRET. Including the FRET deactivation process in the simulation of the decay curves (see Supporting Information) leads to a significant shortening of the lifetime of the excited state, as shown in Figure 11. The energy-selection criterion used to approximate the effect of the variable spectral overlap on the FRET rate (as outlined in the Supporting Information) led to 37% of the snapshots being rejected; 2611 snapshots remained for rotamer 1 and 1862 for rotamer 2. These were used to simulate the decay curves shown and discussed below.

Most studies of FRET have assumed that donor and acceptor can undergo unrestricted isotropic motion, which gives an average κ^2 of 2/3. This assumption is appropriate for studies of solvated chromophores, but not for those restricted within a protein environment. In our case, the mean value of κ^2 for the whole MD trajectory (after applying the energy-selection criterion) is 0.36, indicating that donor and acceptor cannot rotate freely, which is the expected result. Rotamer 1 (snapshot range 1005−5350) gives a lower (0.25) and rotamer 2 a higher (0.51) κ^2 mean value than that obtained for the whole trajectory, although both are lower than the isotropic value. Figure 12 shows the histogram of the orientation factors of the whole trajectory as well as the κ^2 histograms of the two rotamers.

We next calculated FRET rate constants for each snapshot according to eq 14 in the Supporting Information. Modulation with r^{-6} does not change the form of the histograms significantly. Again, Figure 13 shows the histogram of the FRET rate constants of all snapshots for the whole trajectory and for the two rotamers. Rotamer 1 has smaller and rotamer 2 larger relative FRET rate constants.

It is especially interesting to note that only 30% of the variation in the FRET probability is caused by the variation in the distance (33−35 nm) between the two chromophores and 70% by the orientation factor, which varies by a factor of 2.

The decay curve (calculated using eq 15 in the Supporting Information) for all selected MD snapshots is shown in Figure 11 and Figure 14. Table 3 shows that multiexponential fits are not only most appropriate in the case of the whole MD trajectory (2 rotamers) but also if the two rotamers are analyzed independently. A comparison of the mono, bi, and triexponential fits to the decay curves calculated for the whole MD trajectory and the two rotamers is given in Table 3. The values of the weighted (according to the number of snapshots per rotamer)

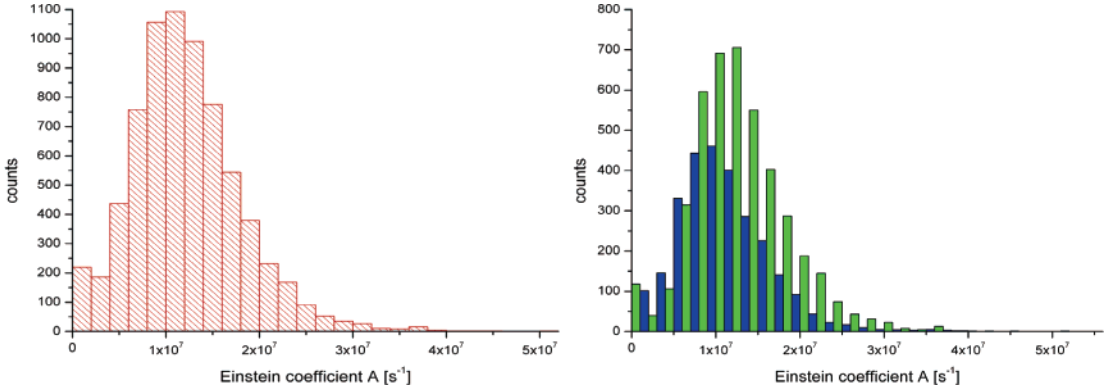

Figure 8. Distribution of Einstein coefficients ($\equiv k_r$) of spontaneous fluorescence emission calculated for Trp43 in TetR. Left (red): Data represents the whole trajectory (2 rotamers, mean value 1.22×10^7). Right: rotamer 1 (green) and rotamer 2 (blue) of Trp43.

Table 2. Parameters Obtained from the Levenberg−Marquardt Fits (Eq 16 in the Supporting Information) of the Calculated Fluorescence Decays of Trp43 in TetR Without FRET Quenching[a]

	whole trajectory (rotamer 1 and 2)			rotamer 1			rotamer 2		
	number of exponentials								
parameter	1	2	3	1	2	3	1	2	3
χ_r^2	2.00×10^{-5}	7.23×10^{-12}	8.40×10^{-14}	2.00×10^{-5}	3.90×10^{-12}	8.46×10^{-14}	3.00×10^{-5}	1.50×10^{-11}	8.46×10^{-14}
r^2	1.00	1.00	1.00	1.00	1.00	1.00	1.00	1.00	1.00
τ_1/ns	4.65	4.74	4.79	4.63	4.72	4.77	4.70	4.77	4.82
τ_2/ns		4.45	4.58		4.44	4.57		4.44	4.60
τ_3/ns			4.25			4.28			4.18
α_1	99.98	70.62	41.09	99.98	68.88	40.43	99.98	78.18	48.44
α_2		29.38	54.63		31.12	54.25		21.82	48.98
α_3			4.28			5.32			2.59

[a] Fluorescence emission and nonradiative deactivation pathways are considered but not FRET. A value of 2×10^8 s^{-1} was assumed for k_{nr} to give approximately the correct overall decay kinetics.[26,28,64−66]

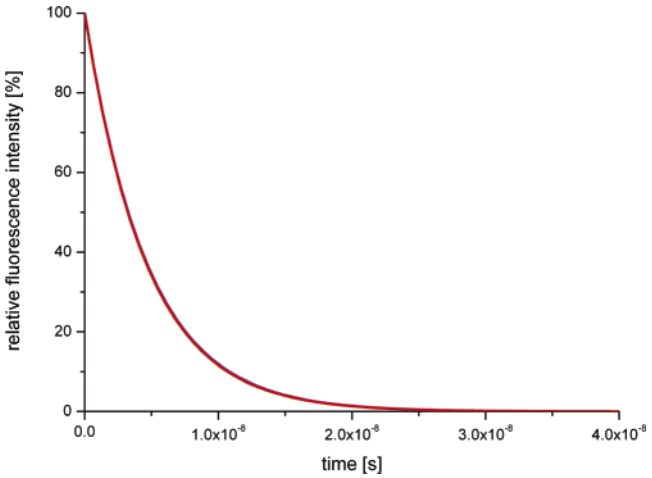

Figure 9. Superimposition of the monoexponential fits to the calculated Trp43 fluorescence decays. (Fluorescence emission and nonradiative deactivation pathways are considered, but not FRET). Red: whole MD trajectory (contains both rotamers of Trp43), hidden by red curve: green: rotamer 1, blue: rotamer 2 of Trp43. A value of 2×10^8 s^{-1} was assumed for k_{nr} to give approximately the correct overall decay kinetics.[26,28,64−66]

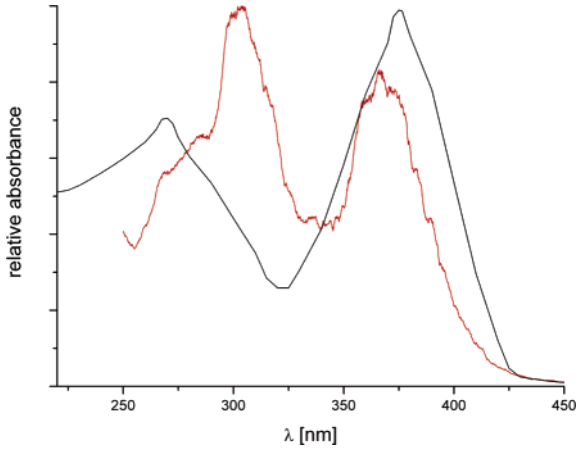

Figure 10. Calculated absorption profile (summed vertical transitions for the ensemble, red) of $[TcMg]^+$ in the protein binding site (QM/MM calculations) and experimental absorption spectrum of $[TcMg]^+$ in water (black, according to ref 71).

averages of the lifetimes of the two rotamers are very close to the fitted values obtained for the total, as shown in Table 3. Thus, we can conclude that all three simulated decay curves (for the total trajectory, for rotamer 1, and for rotamer 2) give equally good justifications for triexponential fits. Thus, lifetimes assignable to individual rotamers are not given by multiexponential fits to fluorescence-decay curves. Rather, the distribution of FRET rates leads to multiexponential fits and for any given number of exponentials, the fitted lifetimes are approximately the population-weighted averages of the values that would be observed for the individual rotamers.

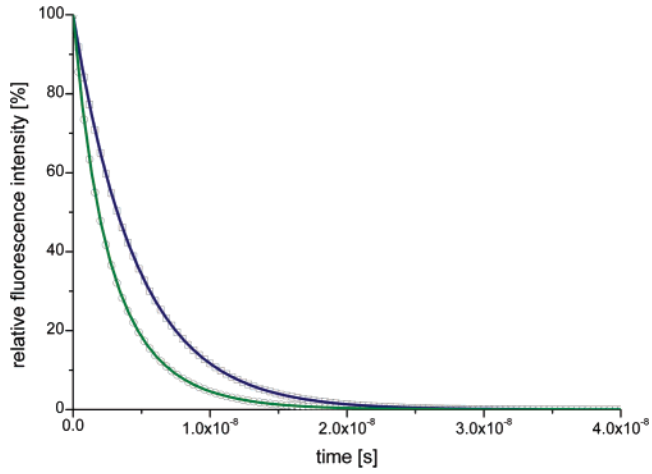

Figure 11. Fits of the simulated fluorescence decays of Trp43. Data represents both rotamers of Trp43. Dark blue: fluorescence emission and nonradiative deactivation pathways are considered, but not FRET (monoexponential fit, see text). Dark green: additionally, FRET quenching is taken into account (triexponential fit required, see text). Gray boxes/circles: actual data points of the simulated decays (only every 100th data point shown for clarity). A value of 2×10^8 s^{-1} was assumed for k_{nr} to give approximately the correct overall decay kinetics.[26,28,64−66]

As noted above, this conclusion rests on the assumption that nonradiative processes can be modeled using a single rate constant. Our results show that FRET can explain multiexponential decay curves but not that FRET is the only possible cause for such behavior. To demonstrate this unequivocally, we would also need to simulate the nonradiative decay processes, a task that is outside the scope of this study.

The values of the longest lifetimes obtained from the fits are around 15% shorter than the value (2×10^{-8} s^{-1} or $\tau = 5$ ns) used for k_{nr}. The mean values of the FRET rate constants k_T for rotamers 1 and 2 are 1.54×10^8 and 2.65×10^8 s^{-1} ($\tau =$ 6.5 and 3.8 ns), respectively. These values would result in calculated distances between the FRET chromophores of 38.6 and 35.3 Å, respectively, if the "isotropic" value of $\kappa^2 = 2/3$ had been used. The mean values of the interchromophore distances for rotamers 1 and 2 from the simulations are 32.9 and 34.0 Å, respectively. Rotamer 1 has smaller κ^2 values (mean value: 0.25) and, consequently, smaller relative FRET rate

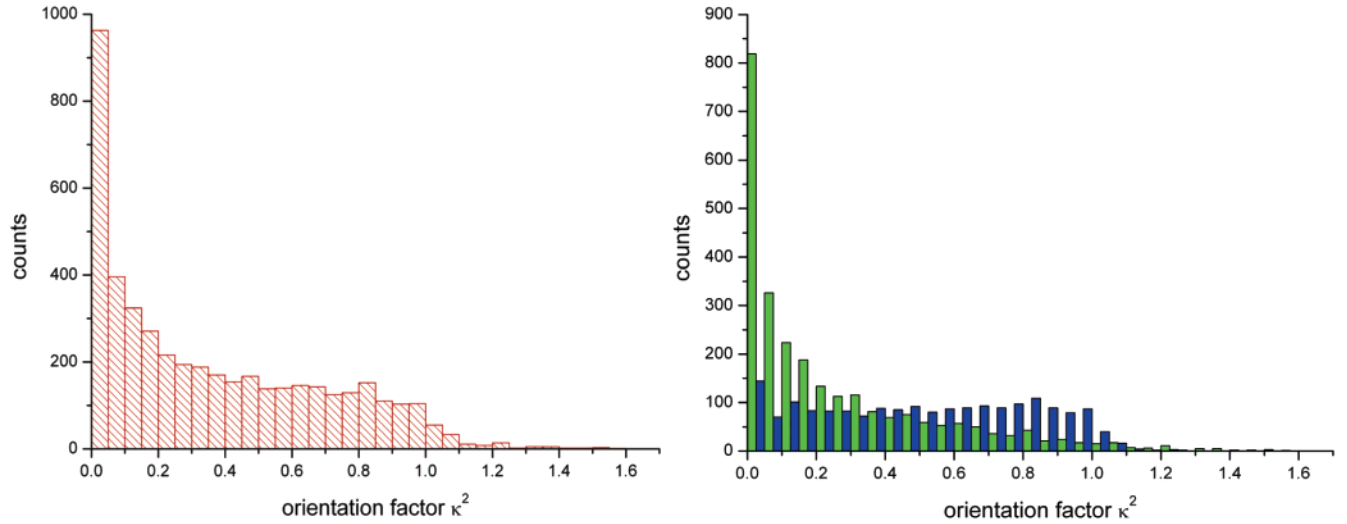

Figure 12. Calculated orientation factors. Left (red): data represents the whole trajectory (snapshots 1−7093) with both rotamers of Trp43 (mean $\kappa^2 = 0.36$). Right: green: rotamer 1 (snapshot range 1005−5350, mean $\kappa^2 = 0.25$), blue: rotamer 2 (snapshots 1−1004 and 5351−7093, mean $\kappa^2 = 0.51$) of Trp43.

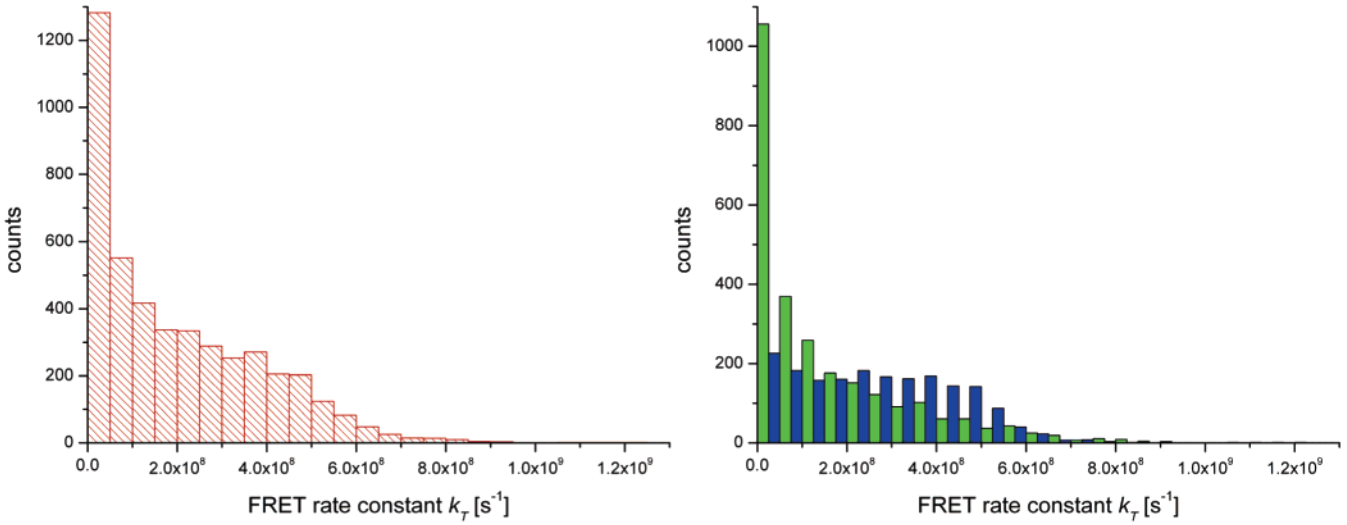

Figure 13. Calculated FRET rate constants k_T. Left (red): data represents the whole trajectory (snapshot range 1−7093) with both rotamers of Trp43. Right: green: rotamer 1 (snapshot range 1005−5350, mean value 1.54×10^8 s^{-1}), blue: rotamer 2 (snapshot range 1−1004 and 5351−7093, mean value 2.65×10^8 s^{-1}) of Trp43. The relative rate constants of each snapshot were multiplied with a factor of 7.69×10^{17} to obtain a rate constant distribution with a mean k_T value of 2×10^8 s^{-1} for the whole trajectory (2 rotamers), which agrees well with experimental work.[26,28,64−66] A value of 2×10^8 s^{-1} was assumed for k_{nr} to give approximately the correct overall decay kinetics.[26,28,64−66]

Table 3. Parameters Obtained from the Levenberg−Marquardt Fits (Eq 16 in the Supporting Information) of the Calculated TetR Trp43 Fluorescence Decays[a]

	whole trajectory (rotamers 1 and 2)			rotamer 1			rotamer 2			weighted average of the rotamers		
	number of exponentials											
parameter	1	2	3	1	2	3	1	2	3	1	2	3
χ_r^2	0.45	4.60×10^{-4}	9.84×10^{-7}	0.36	5.20×10^{-4}	1.26×10^{-6}	0.36	2.90×10^{-4}	3.18×10^{-7}			
r^2	1.00	1.00	1.00	1.00	1.00	1.00	1.00	1.00	1.00			
τ_1/ns	3.02	3.94	4.25	3.31	4.03	4.28	2.50	3.65	4.11	2.97	3.87	4.21
τ_2/ns		1.74	2.45		1.76	2.52		1.70	2.40		1.73	2.47
τ_3/ns			1.36			1.28			1.46			1.36
α_1	95.74	56.82	41.32	96.08	66.45	50.97	96.37	41.05	23.73			
α_2		43.03	40.09		33.39	36.73		58.84	43.99			
α_3			18.58			12.29			32.28			

[a] Fluorescence emission, nonradiative deactivation and fluorescence quenching by FRET are considered. A value of 2×10^8 s^{-1} was assumed for k_{nr} to give approximately the correct overall decay kinetics.[26,28,64−66]

constants than rotamer 2 (κ^2 mean value: 0.51). This results in the "isotropic" value for the distance for rotamer 1 being 5.7 Å longer than that calculated from the snapshot geometries, whereas the difference is only 1.3 Å for rotamer 2. Coincidentally, in this case, both rotamers have average values for κ^2 smaller than 2/3. It is, however, equally possible that the mean

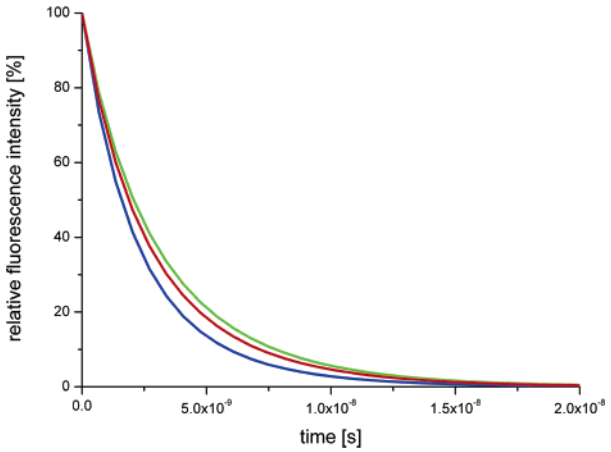

Figure 14. Triexponential fits to the calculated Trp fluorescence decays. Fluorescence emission, nonradiative deactivation, and fluorescence quenching by FRET are considered. Red: whole MD trajectory (contains both rotamers of Trp43), green: rotamer 1, blue: rotamer 2 of Trp43. A value of 2×10^8 s^{-1} was assumed for k_{nr} to give approximately the correct overall decay kinetics.[26,28,64−66]

alignment of rotamers is such that the averaged κ^2 value is larger than 2/3, which would result in an underestimation of the distance using the "anisotropic" value.

Conclusions

Our simulations show the existence of discrete tryptophan rotamers in the TetR/Tc system and, therefore, provide an ideal opportunity to investigate the hypotheses inherent in the rotamer model commonly used to interpret FRET results. Note that we have not attempted to simulate experimental curves exactly but rather have used reasonable values for the rate constants of nonradiative processes that give good agreement for the overall fluorescence decay rates. Direct comparison with experiment therefore largely tests the appropriateness of the assumed nonradiative rate constant. Our conclusions support the existence of tryptophan rotamers with distinctly different rates for Förster energy transfer to tetracycline in the TetR/Tc complex. However, the experimentally observed multiexponential decay curves are not direct evidence for the existence of these rotamers. Thus, the simulations suggest that:

- The observed multiexponential fluorescence-decay curves observed for tryptophan in water must be caused by multiple nonradiative processes and may therefore not be directly related to the situation in proteins. The distribution of geometries in the ensemble in aqueous solution does not cause multiexponential behavior because of the varying fluorescence intensities (Einstein coefficients) alone.
- In TetR/Tc, the inherent fluorescence-decay curves of the individual rotamers without FRET are monoexponential and are very similar for the different rotamers.
- When FRET is taken into account, the individual rotamers do indeed give different fluorescence-decay curves. This variation is caused to a major extent by the relative orientations of the chromophores, not only by the distance.
- However, these individual decay curves are themselves multiexponential because of the width of the distribution of FRET rate constants,[72−74] even for the individual rotamers. The summed ensemble of the rotamers gives a total decay curve that is also multiexponential and in which the fitted lifetimes correspond closely to the weighted averages of those of the individual rotamers.
- Distances calculated from FRET studies may be up to 6 Å in error (in either direction) if the magnitude of the orientation factor κ^2 is assumed to be 2/3 (the value for isotropic solution).

Thus, the experimentally observed multiexponential decay curves are partly the result of the continuous distribution of distances and relative orientations of the two chromophores. The rotamer model is physically correct but is not reflected in the lifetimes obtained from multiexponential fits of fluorescence-decay curves. We are investigating the exact relationship between distance/orientation distributions and fitted decay curves in detail and will report the results shortly.

Acknowledgment. This work was supported by *Sonderforschungsbereich 473*, "Mechanisms of Transcriptional Regulation", financed by the Deutsche Forschungsgemeinschaft, and by the Bayerische Staatsregierung as part of the KONWIHR program.

Supporting Information Available: The Supporting Information (20 pages, print/PDF) gives details of the following aspects of this work: (1) Preparation of the protein simulation system; (2) MD simulations; (3) cutting scheme for semiempirical CI calculations; (4) absorption and emission profiles; (5) fluorescence-resonance-energy-transfer (FRET) probabilities; (6) fitting decay curves; (7) references abbreviated in text. This material is available free of charge via the Internet at http://pubs.acs.org.

JA058414L

(70) *Jmol*, version 5; http://jmol.sourceforge.net, 2001.
(71) Schneider, S. In *Tetracyclines in Biology, Chemistry and Medicine;* Nelson, M., Hillen, W., Greenwald, R. A., Eds.; Birkhäuser Verlag: Basel, Boston, Berlin, 2001; pp 65−104.
(72) Alcala, J. R.; Gratton, E.; Prendergast, F. G. *Biophys. J.* **1987**, *51*, 925−936.
(73) James, D. R.; Ware, W. R. *J. Phys. Chem.* **1985**, *89*, 5450−5458.
(74) Engh, R. A.; Chen, L. X.-Q.; Fleming, G. R. *Chem. Phys. Lett.* **1986**, *126*, 365−372.